Roebling Suspension Bridge. I: Finite-Element Model and Free Vibration Response

Wei-Xin Ren[1]; George E. Blandford, M.ASCE[2]; and Issam E. Harik, M.ASCE[3]

Abstract: This first part of a two-part paper on the John A. Roebling suspension bridge (1867) across the Ohio River is an analytical investigation, whereas Part II focuses on the experimental investigation of the bridge. The primary objectives of the investigation are to assess the bridge's load-carrying capacity and compare this capacity with current standards of safety. Dynamics-based evaluation is used, which requires combining finite-element bridge analysis and field testing. A 3D finite-element model is developed to represent the bridge and to establish its deformed equilibrium configuration due to dead loading. Starting from the deformed configuration, a modal analysis is performed to provide the frequencies and mode shapes. Transverse vibration modes dominate the low-frequency response. It is demonstrated that cable stress stiffening plays an important role in both the static and dynamic responses of the bridge. Inclusion of large deflection behavior is shown to have a limited effect on the member forces and bridge deflections. Parametric studies are performed using the developed finite-element model. The outcome of the investigation is to provide structural information that will assist in the preservation of the historic John A. Roebling suspension bridge, though the developed methodology could be applied to a wide range of cable-supported bridges.

DOI: 10.1061/(ASCE)1084-0702(2004)9:2(110)

CE Database subject headings: Bridges, suspension; Finite element method; Three-dimensional models; Vibration; Natural frequency; Dead load; Equilibrium; Model analysis.

Introduction

Many of the suspension bridges built in the United States in the 19th Century are still in use today but were obviously designed for live loads quite different from the vehicular traffic they are subjected to today. A good example is the John A. Roebling suspension bridge, completed in 1867, over the Ohio River between Covington, Kentucky, and Cincinnati, Ohio. To continue using these historic bridges, it is necessary to evaluate their load-bearing capacity so that traffic loads are managed to ensure their continued safe operation (Spyrakos et al. 1999). Preservation of these historic bridges is important since they are regarded as national treasures.

The unique structural style of suspension bridges permits longer span lengths, which are aesthetically pleasing but also add to the difficulties in performing accurate structural analysis. Design of the suspension bridges built in the early 19th Century was based on a geometrically linear theory with linear-elastic stress-strain behavior. Such a theory is sufficiently accurate for shorter spans or for designing relatively deep, rigid stiffening systems that limit the deflections to a small fraction of the span length. However, a geometrically linear theory is not well adapted to the design of suspension bridges with long spans, shallow trusses, or a large dead load. A more exact theory is required that takes into account the deformed configuration of the structure.

In modern practice, finite-element (FE) analysis is effective in performing the geometric nonlinear analysis of suspension bridges. Geometric nonlinear theory can include the nonlinear effects inherent in suspension bridges: cable sags, large deflections, and axial force and bending moment interaction with the bridge stiffness. Two- or three-dimensional finite-element (FE) models with beam and truss elements are often used for both the superstructure and the substructure of cable-supported bridges (Nazmy and Abdel-Ghaffar 1990; Wilson and Gravelle 1991; Lall 1992; Ren 1999; Spyrakos et al. 1999).

Another area where FE analysis has had a major impact regarding suspension bridge analysis is in predicting the vibration response of such bridges under wind, traffic, and earthquake loadings (Abdel-Ghaffar and Rubin 1982; Abdel-Ghaffar and Nazmy 1991; Boonyapinyo et al. 1999; Ren and Obata 1999). In addition, major efforts have been expended to predict the lateral (Abdel-Ghaffar 1978), torsional (Abdel-Ghaffar 1979), and vertical (Abdel-Ghaffar 1980) vibrations of suspension bridges to predict their dynamic behavior. FE parametric studies (West et al. 1984) have demonstrated the variation in the modal frequencies and shapes of stiffened suspension bridges.

Structural evaluations using dynamics-based methods have become an increasingly utilized procedure for nondestructive testing (Friswell and Mottershead 1995; Brownjohn and Xia 2000). A difficulty with dynamics-based methods is establishing an accurate FE model for the aging structure. FE models typically pro-

[1]Professor, Dept. of Civil Engineering, Fuzhou Univ., Fuzhou, Fujian Province, People's Republic of China; and Professor, Dept. of Civil Engineering, Central South Univ., Changsha, Hunan Province, People's Republic of China. E-mail: renwx@yahoo.com

[2]Professor, Dept. of Civil Engineering, Univ. of Kentucky, Lexington, KY 40506-0281.

[3]Professor, Dept. of Civil Engineering, Univ. of Kentucky, Lexington, KY 40506-0281 (corresponding author). E-mail: iharik@engr.uky.edu

Note. Discussion open until August 1, 2004. Separate discussions must be submitted for individual papers. To extend the closing date by one month, a written request must be filed with the ASCE Managing Editor. The manuscript for this paper was submitted for review and possible publication on November 28, 2001; approved on November 19, 2002. This paper is part of the ***Journal of Bridge Engineering***, Vol. 9, No. 2, March 1, 2004. ©ASCE, ISSN 1084-0702/2004/2-110–118/$18.00.

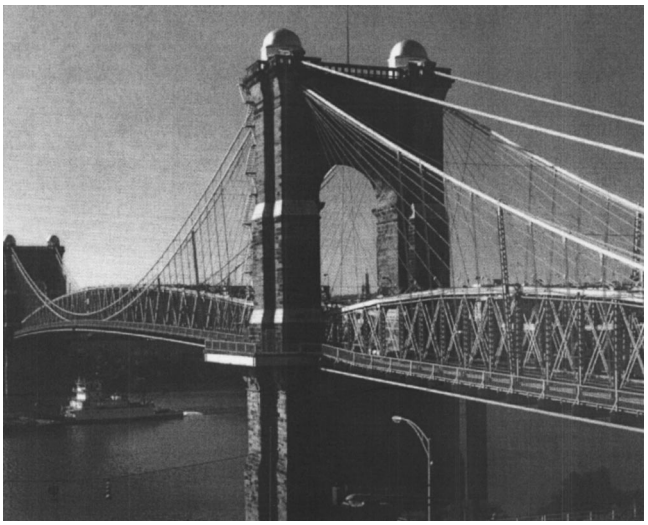


Fig. 1. John A. Roebling suspension bridge

vide dynamic performance predictions that exhibit relatively large frequency differences when compared with the experimental frequencies and, to a lesser extent, the models also predict differences in the modes of response. These differences come not only from the modeling errors resulting from simplified assumptions made in modeling the complicated structures, but also from parameter errors due to structural damage and uncertainties in material and geometric properties. Dynamics-based evaluation is therefore based on a comparison of the experimental modal analysis data obtained from in situ field tests with the FE predictions. To improve the FE predictions, the FE model must be realistically updated (calibrated) to produce the experimental observed dynamic measurements (Friswell and Mottershead 1995). Thus the scope of this study on the dynamics-based evaluation of the Roebling suspension bridge is composed of several tasks: FE modeling, modal analysis, in situ ambient vibration testing, FE model updating, and bridge capacity evaluation under live loading.

This paper presents the results of the first two tasks in the dynamics-based evaluation scheme of the Roebling suspension bridge. A 3D FE model is developed for the *ANSYS* (1999) commercial FE computer program. All the geometric nonlinear sources discussed previously are included in the model. A static dead-load analysis is carried out to achieve the deformed equilibrium configuration. Starting from this deformed configuration, a modal analysis is performed to provide the frequencies and mode shapes that strongly affect the free vibration response of the bridge. Parametric studies are performed to determine the significant material and structural parameters. Results of the FE modal analysis are compared with ambient vibration measurements in the accompanying paper (Ren et al. 2004). This FE model, after being updated (calibrated) based on the experimental measurements, will serve as the baseline for the structural evaluation of the bridge. The baseline structural evaluations provide important design information that will assist in the preservation of the Roebling suspension bridge, and furthermore, the methodology developed in these two papers can be applied to a wide range of historic cable-supported bridges.

Bridge Description and Historic Background

The John A. Roebling suspension bridge, shown in Fig. 1, carries KY 17 over the Ohio River between Covington, Kentucky, and Cincinnati, Ohio. The 321.9 m (1,056 ft) main span of the suspension bridge carries a two-lane, 8.53 m (28 ft) wide steel grid deck roadway with 2.59 m (8 ft 6 in.) wide sidewalks cantilevered from the trusses. The towers are 73.15 m (240 ft) tall and 25×15.85 m (82×52 ft) at their base and encompass 11,320 m^3 (400,000 cu ft) of masonry. Towers bear on timber mat foundations that are 33.53×22.86 m (110×75 ft) and 3.66 m (12 ft) thick. The suspension bridge system is composed of two sets of suspension cables restrained by massive masonry anchorages. Stay cables radiate diagonally from the towers to the upper chords of the stiffening trusses. Deck loads are transferred from the stringers and floor beams to the suspenders, trusses, and stays and then to the suspension cables, which then transfer the loads to the anchorages and towers. The approach span roadway varies from 6 to 7.25 m (20 to 24 ft) wide and is composed of a concrete deck supported by riveted steel plate girders. The plan and elevation views of the Roebling suspension bridge are shown in Fig. 2.

The John A. Roebling suspension bridge (completed in 1867) was the first permanent bridge to span the Ohio River between

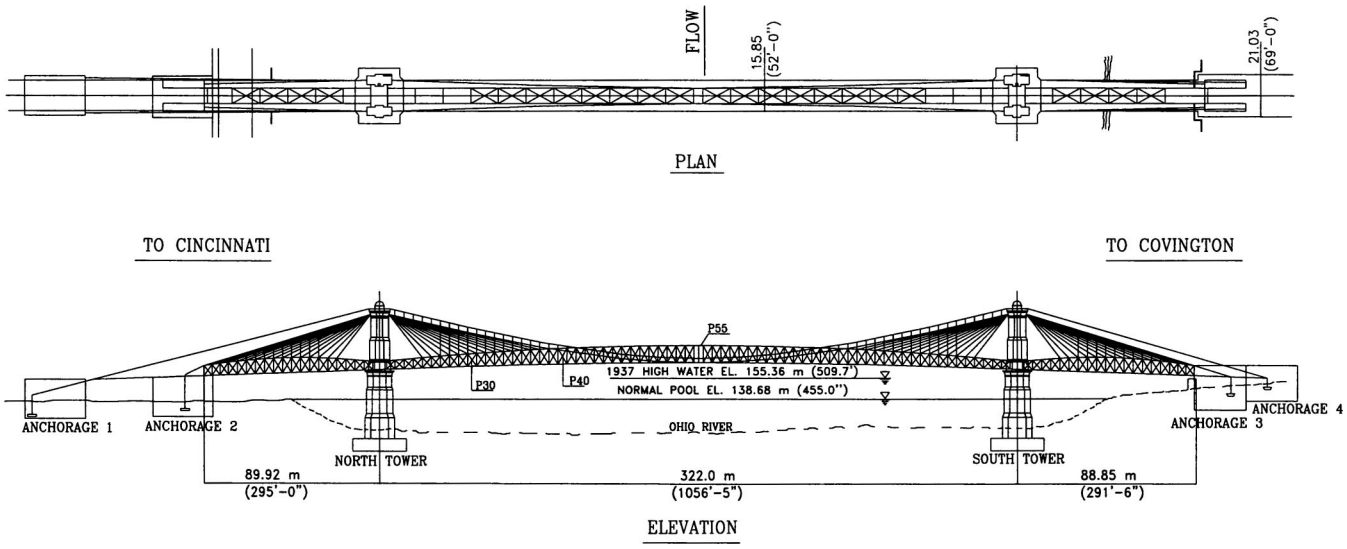


Fig. 2. Layout of Roebling suspension bridge

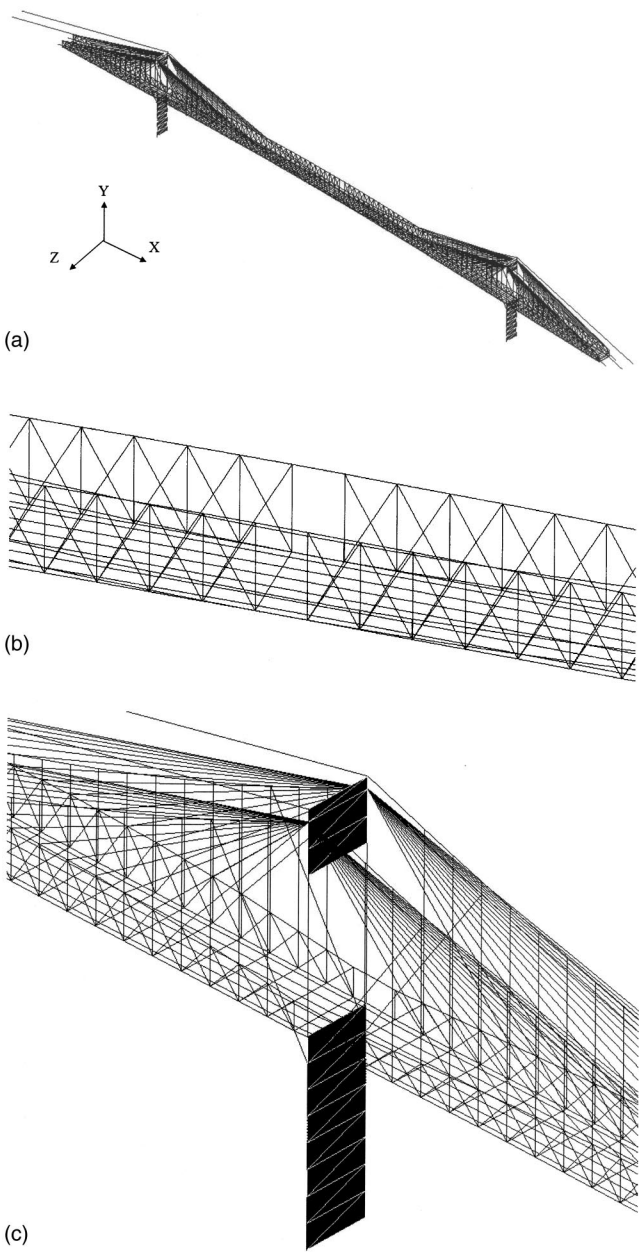


Fig. 3. 3D finite-element model of Roebling bridge: (a) full 3D elevation; (b) part 3D elevation (span center and stiffness truss); (c) part 3D elevation (tower and cables)

Covington and Cincinnati. At the time of its opening, the soaring masonry towers represented a new construction method that supported a state-of-the-art iron-wire cable technology. This monument to civil engineering of the 1800s represented the longest span in the world at the time of its opening. Today, this nationally historic bridge (designated as such in 1975) remains the second longest span in Kentucky, and after 133 years of service, the bridge still carries average daily traffic of 21,843 vehicles (Parsons et al. 1988). The bridge is currently posted at 133.4 kN (15 t) for two-axle trucks and 97.9 kN (22 t) for three-, four-, and five-axle trucks.

Finite-Element Modeling

For the purposes of this study, a complete 3D FE model has been developed as shown in Fig. 3(a). This model is used for both static and dynamic analyses. The FE model of the Roebling suspension bridge is briefly described herein, with greater details provided in Ren et al. (2003).

Element Types

A suspension bridge is a complex structural system in which each member plays a different role. In the FE model, four types of FEs used to model the different structural members: main cables and suspenders, stiffening trusses, floor beams and stringers, and towers.

All cable members of the Roebling suspension bridge (primary cables, secondary cables, suspenders, stay cables, and stabilizer cables) are designed to sustain tension force only and are modeled using a single 3D tension-only truss element between joints [Fig. 3(c)], which allows for the simulation of slack compression cables. Both stress stiffening and large displacement modeling are available. Stress stiffening modeling is needed for the cables since cable stiffness is dependent on the tension force magnitude. Cable sag can also be modeled within the stress stiffening modeling. An important input parameter is the initial element strain, which is used in calculating the initial stress stiffness matrix.

The stiffening truss is modeled as a 3D truss composed of a single beam or truss element between joints [Fig. 3(b)]. Top and bottom chords of the truss are modeled as 3D elastic beam elements since they are continuous across many panels. Vertical truss members are also modeled as 3D elastic beam elements, whereas the diagonals are modeled as 3D truss elements since they are pinned connected and do not provide much bending stiffness. Tie rods that connect the primary and secondary cables are also modeled as 3D truss elements.

Tower columns are modeled as 3D elastic beam elements, whereas the web walls of towers above and below the deck are modeled as three-node quadrilateral membrane shell elements, as shown in Fig. 3(c), because the bending of these walls is of secondary importance.

The deck is simplified as stringers and floor beams in the analytical model; that is, the principal load-bearing structural elements of the deck are the stringers and floor beams. These can be subjected to tension, compression, bending, and torsion, and consequently each one is modeled using a single 3D elastic beam element between joints. Three-dimensional FE discretization of the Roebling suspension bridge consists of 1,756 nodes and 3,482 elements, resulting in 7,515 active degrees of freedom.

Material and Cross-Section Properties

Basic materials used in the Roebling suspension bridge are structural steel, masonry towers, and iron cables. The material constants used are summarized in Table 1. Note that the stringer and floor beam mass densities include the contribution from the bridge deck weight and sidewalks, as well as the lateral bracing system contribution.

In addition to the material properties of Table 1, cross-sectional properties and initial strains are required. Cross-sectional constants are used to model the structural member features described below:

- Stiffening truss: Top chord is a built-up member with a solid cover plate, and bottom chord is a built-up member with top and bottom lacing bars. The top and bottom chords have riveted joints but employ pin connections at each panel point for the verticals, which are latticed columns. Diagonals are steel eye bars.

Table 1. Material Properties

Group number	Young's modulus [MPa (lb/ft^2)]	Poisson's ratio	Mass density [kg/m^3 (lb/ft^3)]	Structural member
1	2.1×10^5 (4.386×10^9)	0.30	7,849 (490)	Stiffening trusses
2	2.0×10^5 (4.177×10^9)	0.30	7,849 (490)	Cables
3	2.0×10^5 (4.177×10^9)	0.30	7,849 (490)	Suspenders
4	2.0×10^5 (4.177×10^9)	0.30	7,849 (490)	Stay wires and tie rods
5	2.0×10^4 (4.177×10^8)	0.15	2,500 (156)	Tower
6	2.1×10^5 (4.386×10^9)	0.30	19,575 (1,222)	Floor beams and stringers

- Primary cables: Composed of seven strands, each containing 740 No. 9 gauge cold-blast charcoal iron wires, for a total of 5,180 wires. These wires are parallel to each other and form a cable that is 313.27 mm (12 1/3 in.) in diameter with an effective area of 55,920 mm^2 (86.67 in.^{2}). A total of 4,671.2 kN (1,050.2 kips) of cable wire was used, which also includes the wrapping wire. Design ultimate strength of one wire is 7,206 N (1,620 lb); therefore the design ultimate strength per primary cable is 37,326 kN (8,391.6 kips).
- Secondary cables: Composed of 21 strands, including 7 that contain 134 wires each and 14 that contain 92 wires each, resulting in 2,226 wires. These No. 6 gauge ungalvanized steel wires are parallel to each other and form a cable that is 266.7 mm (10.5 in.) in diameter, resulting in an effective area of 43,086 mm^2 (66.78 in.^{2}). Design ultimate strength of one wire is approximately 24,000 N (5,400 lb). Therefore, the design ultimate strength per cable is 53,467 kN (12,020 kips).
- Suspenders: Composed of three helical wire ropes in which the outer pair of wrought iron wire ropes is 38.1 mm (1.5 in.) in diameter and is part of the original construction. These pairs of ropes at 1.52 m (5 ft) spacing supported the original truss and floor system. In 1897, a third rope 57.1 mm (2 1/4 in.) in diameter was added, and these additional ropes are spaced at 4.57 m (15 ft) intervals. The combined ultimate strength is 2,517.6 kN (566 kips).
- Stay wires: There are 72 stay cables. These stays are 57.1 mm (2 1/4 in.) diameter, helical iron wire ropes with an ultimate strength of 8,000 kN (1,800 kips) each.
- Floor beams and stringers: In the suspension span, each 127 mm (5 in.) open steel grid deck is supported by C10×20 crossbeams spaced at 1.143 m (3 ft 9 in.), resting on six stringers spaced at approximately 1.6 m (5 ft 3 in.). The four outermost stringers are 381 mm (15 in.) I-sections that weigh 729.5 N/m (50 lb/ft), and the two center stringers are 508 mm (20 in.) I-sections that weigh 948.4 N/m (65 lb/ft). Floor beams are riveted, built-up steel sections with a web plate 914.4 mm (36 in.) deep with four flange angles riveted to it.

Boundary Conditions

The towers of the Roebling suspension bridge are modeled as fixed at the base, whereas the cable (both primary and secondary) ends are modeled as fixed at the anchorages. The stiffener truss and stringer beams are assumed to have a hinge support at the left and right masonry supports but they are continuous at the towers to simulate the actual structure. In addition, the stiffener truss for the Roebling suspension bridge is an uncommon one-hinge design placed in the center of the span to provide for temperature expansion. The hinge was modeled by defining separately coincident nodes in the top as well as the bottom chords at the midspan. Coupling the vertical and transverse displacements of the coincident nodes while permitting them to move independently in the horizontal direction simulates the expansion hinge effect. In addition, the twisting and in-plane rotations are constrained to displace equally, but the rotation about the lateral (z-axis) of the bridge is discontinuous.

Static Analysis—Dead Load

In the design of suspension bridges, the dead load often contributes most of the loading. It was realized as early as the 1850s that the dead load has a significant influence on the stiffness of a suspension bridge. In the FE analysis, this influence can be included through static analysis under dead loading before the live load or dynamic analysis is carried out. The objective of the static analysis process is to achieve the deformed equilibrium configuration of the bridge due to dead loads in which the structural members are prestressed.

For the static analysis of the Roebling suspension bridge under dead loading, the value of the deck dead load is taken to be 36.49 kN/m (2,500 lb/ft), which is taken from the report by Hazelet and Erdal (1953). In the FE model, the dead load is applied directly on each node of both inner stringers. The distributed load is equivalent to a 166.81 kN (37.5 kips) point load applied on each node of the inner stringers.

Table 2. Influence of Cable Prestrain on Maximum Axial Forces and Main-Span Deflections

	Bottom chord (kN)		Top chord (kN)		Cable members (kN)			
Prestrain	Panel 30	Panel 55	Panel 40	Panel 55	Primary cable	Secondary cable	Suspender	Deflection (m)
0.0	−1,771.0	720.4	2,830.8	−37.5	6,992.7	5,004.9	101.6	0.967
0.1×10^{-5}	−1,769.0	719.8	2,827.6	−37.4	6,996.7	5,006.6	101.6	0.966
0.1×10^{-4}	−1,718.0	713.6	2,799.0	−37.1	7,028.7	5,033.4	102.1	0.956
0.1×10^{-3}	−1,574.9	651.3	2,514.1	−33.4	7,351.2	5,292.7	107.2	0.859
0.5×10^{-3}	−794.7	367.2	1,259.5	0.0	8,773.7	6,452.7	129.7	0.431
0.6×10^{-3}	−600.6	295.8	951.2	−12.6	9,130.9	6,745.4	135.4	0.325
0.7×10^{-3}	−406.8	224.6	645.8	−8.2	9,489.8	7,044.3	141.1	0.221
0.8×10^{-3}	−213.8	153.6	343.7	−3.7	9,850.5	7,336.1	146.8	0.118

Note: One panel=4.572 m (15 ft).

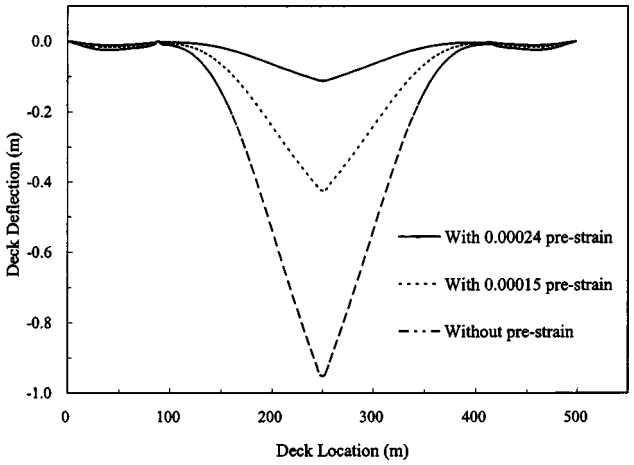


Fig. 4. Main-span deck deflections for various cable prestrain levels

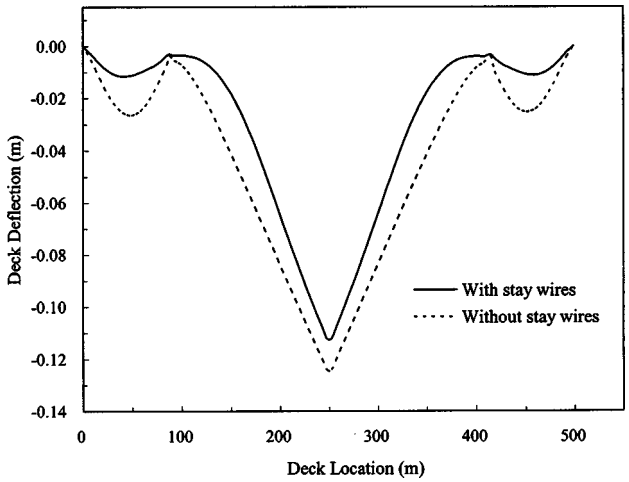


Fig. 5. Main-span deck deflections with and without stay wires

Initial Tension in Main Cables

A cable-supported bridge directly derives its stiffness from cable tension. For a completed suspension bridge, the initial position of the cable and bridge is not known; only the final geometry of the bridge due to the dead loading is known. The initial bridge geometry has been modeled based on the dead-load deflected shape of the bridge. When the bridge is erected, the truss is initially unstressed. The dead load is borne completely by the cables, which is a key assumption. It turns out that the ideal FE model of a suspension bridge should be such that on application of the dead load, the geometry of the bridge does not change, since this is indeed the geometry of the bridge. Furthermore, no forces should be induced in the stiffening structure. This can be approximately realized by manipulating the initial tension force in the main cable that is specified as an input prestrain in the cable elements. The initial tension in the cables can be achieved by trial and error until a value is found that leads to minimum deck deflection and minimum stresses in the stiffening trusses.

The maximum axial force and main span deflection variations versus cable prestrain are summarized in Table 2. Panel locations for panels 30, 40, and 55 are shown in Fig. 2 as P30, P40, and P55, respectively. Deck deflection profiles for varying prestrains in the cables are plotted in Fig. 4. It is clear that the deck deflections and the forces in the stiffening truss decrease with increasing cable prestrain, whereas forces in the cables and suspenders increase with increasing cable prestrain. It is observed that smaller cable prestrain (below 0.1×10^{-3}) has almost no effect on the deflections and forces of the bridge.

It is evident that for a prestrain of 0.8×10^{-3} in both primary and secondary cables the deflections of the deck are nominal. In the computer model, the deck deflections cannot be reduced further by increasing the prestrain without causing an upward deflection of the deck at some points. Although the maximum deflection at the deck center with a prestrain of 0.8×10^{-3} in both primary and secondary cables is about 118.9 mm (4.68 in.), it is considered an adequate simulation of the dead-load deflected shape of the bridge. Even though this leads to initial stresses in the stiffening truss, the magnitude of the stresses is reduced to a minimum since the cables carry most of the dead load, as is evident from the forces in the suspenders. The presence of initial stresses in the truss model is conservative as far as estimating the capacity of the truss.

With cable prestrain of 0.8×10^{-3}, the force in the suspenders of the main span due to dead load alone is typically 146.8 kN (33 kips). This means that of the 166.8 kN (37.5 kips) force applied at each panel point along the bridge deck, 146.8 kN (33 kips) are transferred to the main cable. Thus the use of a prestrain of 0.8×10^{-3} in the primary and secondary cables is about 90% efficient in keeping the truss stress free under gravity loading. In addition, the total (primary plus secondary) cable tension of 17,187 kN (3,864 kips) determined by the computer analysis is close to the 15,568 kN (3,500 kips) reported by Hazelet and Erdal (1953). Therefore, a model with an initial prestrain of 0.8×10^{-3} in the cable elements is considered the correct analytical model.

Another interesting feature of the Roebling suspension bridge is the inclined stays. In the original design, Roebling felt that the use of stays was the most economical and efficient means of providing stiffness to long-span bridges. These stays also carry approximately 10% of the total bridge load (Hazelet and Erdal 1953). Deck deflection comparisons for the model with and without inclined stays are given in Table 3 and Fig. 5. These numerical results demonstrate that the stay wires reduce the central deck

Table 3. Influence of Stays on Maximum Axial Forces and Main-Span Deflections

	Bottom chord (kN)		Top chord (kN)		Cable members (kN)			Deflection (m)	
Stays	Panel 30	Panel 55	Panel 40	Panel 55	Primary cable	Secondary cable	Suspender	Side span	Main span
Without stays	−78.09	37.06	19.22	2.95	10,121	7,585.6	151.53	0.0253	0.1298
With stays	−213.78	153.62	343.72	−3.69	9,851	7,336.1	146.80	0.0116	0.1180

Note: One panel=4.572 m (15 ft).

Table 4. Influence of Deformation Analysis on Axial Forces and Main-Span Deflections Including Cable Prestrain

	Bottom chord (kN)		Top chord (kN)		Cable members (kN)			
Analysis type	Panel 30	Panel 55	Panel 40	Panel 55	Primary cable	Secondary cable	Suspender	Deflection (m)
Small deformation	−213.8	153.6	343.7	−3.69	9,851	7,336	146.8	0.1180
Large deformation	−212.3	159.7	344.1	−3.75	9,864	7,337	146.8	0.1177

Note: One panel=4.572 m (15 ft).

deflection by about 55% in the side spans, but only a 10% reduction is observed in the main span. The results also show that initial strain in the stay wires only contributes slightly to deck deflection reduction. Thus, prestrain in the elements representing the inclined stays is neglected in the analytical model.

An inspection of the axial forces induced in the bottom and top chords of the stiffening truss shows that the force pattern changes along the bridge deck under dead loading. As shown in Table 3, axial force in the bottom chords of the main span goes from compression at the towers to tension at the span center, while the top chords follow the opposite pattern, that is, from tension at the towers to compression at the span center. This force pattern distribution is consistent with the bending-moment distribution of a continuous beam subjected to a gravity load with an internal hinge at the center.

Geometric Nonlinearity

It is well known that a long-span cable-supported bridge exhibits geometric nonlinearity that is reflected in the nonlinear load-deflection behavior. Geometric nonlinear sources include (1) large deflection effect due to changes in geometry; (2) combined axial force and bending moment interaction; and (3) sag effect due to changes in cable tension.

Large deflections can be accounted for by recalculating the stiffness matrices in terms of the updated structural geometry. Large deflection of a structure is characterized by large displacements and rotations but small strains. Interaction between axial force and bending moment can be included through the inclusion of a structure geometric stiffness. Sagging cables require the inclusion of an explicit stress-stiffness matrix in the mathematical formulation in order to provide the numerically stabilizing initial stiffness. Introducing preaxial strains in the cables and then running a static stress-stiffening analysis to determine an equilibrium configuration of the prestressed cables can include cable sag. Stress stiffening is an effect that causes a stiffness change in the element due to the loading or stress within the element. The stress-stiffening capability is needed for analysis of structures for which the stiffness is a function of the tension force magnitude, as is the case with cables.

The FE model described previously is used to determine the large deflection effect on the structural behavior of the Roebling suspension bridge due to dead loading. Table 4 compares the maximum axial forces in typical members and the maximum deck deflection at the span center for small and large deflection analyses. The stress-stiffening capability is included in both analyses to ensure a convergent solution. It is clearly shown that large deflections have almost no effect on the member forces and deck deflection due to dead load alone. This is consistent with the observation that the maximum deck deflection of the bridge is very limited (about 118.9 mm) due to introducing prestrain of 0.8×10^{-3} in the cables, which results in a relatively stiff bridge. Further comparison between small and large deflection analyses without cable prestrain, as shown in Table 5, demonstrates that large deflections do not change the member forces and deck deflection significantly, even though the maximum deck deflection of the bridge reaches about 0.945 m. It can be concluded that the large deflection analysis is not necessary in determining the initial equilibrium configuration of the bridge due to dead load and a small deflection analysis is sufficient, but stress stiffening must be included. However, convergent 3D nonlinear simulation of the Roebling suspension bridge with both primary and secondary cables required a large deflection solution along with the stress-stiffening behavior with convergence determined using displacements.

In the FE modeling of a suspension bridge, the cable between two suspenders is discretized as a single tension-only truss element (cable element). Truss elements are also used to model suspenders and tie rods connecting the primary and secondary cables, which do not provide sufficient restraints at each cable element node in the transverse (lateral or *z*-axis) direction since they are in the $x-y$ plane. This limitation is solved by constraining the transverse displacement of each cable node to equal the transverse displacement of the corresponding node at the bottom chord of the stiffening truss, which should be fairly close to the physical response of the suspension bridge.

Table 5. Influence of Deformation Analysis on Axial Forces and Main-Span Deflections Excluding Cable Prestrain

	Bottom chord (kN)		Top chord (kN)		Cable members (kN)			
Analysis type	Panel 30	Panel 55	Panel 40	Panel 55	Primary cable	Secondary cable	Suspender	Deflection (m)
Small deformation	−1,771	720.4	2,831	−37.47	6,993	5,005	101.6	0.9668
Large deformation	−1679,	795.2	2,856	−35.73	7,083	5,050	102.5	0.9449

Note: One panel=4.572 m (15 ft).

Table 6. Frequency Results

Mode number	Case 1 (Hz)	Case 2 (Hz)	Case 3 (Hz)	Dominant mode
1	0.152	0.191	0.196	1st transverse
2	0.334	0.412	0.420	2nd transverse
3	0.493	0.599	0.614	3rd transverse
4	0.647	0.684	0.686	1st vertical
5	0.714	0.841	0.869	4th transverse
6	0.879	1.032	1.069	5th transverse
7	1.116	1.243	1.246	2nd vertical
8	1.121	1.294	1.336	6th transverse
9	1.294	1.500	1.513	1st torsional
10	1.488	1.515	1.546	Coupled mode
11	1.518	1.571	1.574	3rd vertical
12	1.561	1.782	1.839	7th transverse
13	1.744	1.989	2.008	2nd torsional
14	1.872	2.004	2.051	8th transverse
15	2.031	2.300	2.314	3rd torsional
16	2.232	2.310	2.364	9th transverse

Modal Analysis—Free Vibration

Modal analysis is needed to determine the natural frequencies and mode shapes of free vibration. A shifted Block-Lanczos method (Grimes et al. 1994) in *ANSYS* is chosen to extract the eigenvalue/eigenvector pairs. As mentioned previously, the modal analysis of a suspension bridge should include two steps: static analysis under dead loading, followed by a prestressed modal analysis. To investigate the effect of the static analysis and cable prestrain on the dynamic properties of the Roebling suspension bridge, the following three cases are considered:

- Case 1: Modal analysis without dead load effect based on the undeformed configuration;
- Case 2: Prestressed modal analysis that follows a dead-load linear static analysis, but without the prestrain in the cables; and
- Case 3: Prestressed modal analysis that includes the dead-load linear-static analysis results with a cable prestrain of 0.8×10^{-3}.

A frequency comparison for these three cases is summarized in Table 6, where self-weight is clearly shown to improve stiffness. The frequencies in Table 6 show that the inclusion of self-weight (Case 2) resulted in an increased transverse (lateral) natural frequency of nearly 20%, whereas the increase in the Case 2 versus Case 1 vertical natural frequency was only about 5%. This observation shows that the transverse (lateral) stiffness of the bridge is more significantly impacted than is the vertical stiffness of the bridge. Therefore, modal analyses without a dead-load static analysis will result in the underestimation of the cable-supported bridge capacity.

Comparing Cases 2 and 3 shows that the prestrain in the cables only slightly increased the natural frequencies of the suspension bridge. Thus, it is prestress induced by dead loading, which contributes significant stiffness improvement rather than the initial equilibrium configuration. However, the initial equilibrium configuration is essential in determining the dynamic response under wind or seismic loadings [for example, Abdel-Ghaffar and Nazmy (1991); Ren and Obata (1999)].

Case 3 (prestressed modal analysis starting from the dead-load equilibrium configuration with a prestrain of 0.8×10^{-3} in the cables) is closer to the actual situation and has been implemented here to evaluate the modal properties of the Roebling suspension bridge. Since the bridge is modeled as a complete 3D structure, all possible modes could be obtained. Typical transverse, vertical, and torsional mode shapes are shown in Fig. 6, and a coupled transverse-torsion mode shape is shown in Fig. 7. Table 6 shows that the dominant free vibration modes in the low-frequency (0–1.0 Hz) range are in the transverse direction. This may be explained by the fact that the lateral load-resisting system of the Roebling bridge is a single truss in the plane of the bottom stiffener truss chords (Fig. 2), unlike the lateral systems of modern bridges, which have major lateral load-resisting systems consisting of two lateral trusses. Furthermore, guy wires in the horizontal plane of the lower chords, which were meant to add lateral stability, are slack and thus ineffective.

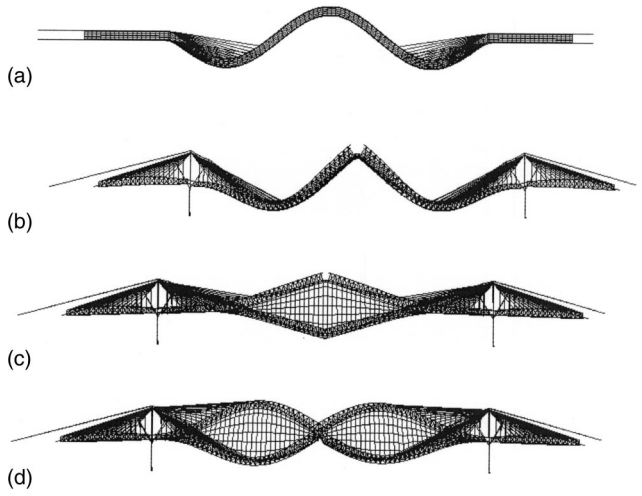


Fig. 6. Some typical vibration modes: (a) plan view of third transverse mode ($f=0.614$ Hz); (b) elevation view of third vertical mode ($f=1.574$ Hz); (c) elevation view of first torsional mode ($f=1.513$ Hz); (d) elevation view of second torsional mode ($f=2.008$ Hz)

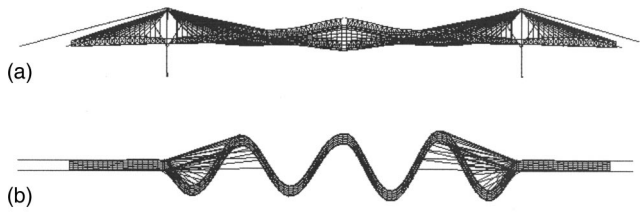


Fig. 7. Transverse/torsional coupled mode ($f=1.546$ Hz): (a) elevation view; (b) plan view

Parametric Studies

As mentioned previously, a major advantage of FE modeling and analysis is in performing parametric studies. Structural and material parameters that may significantly impact the modal properties can be identified through parametric studies. Structural and material parameters of the Roebling suspension bridge include deck

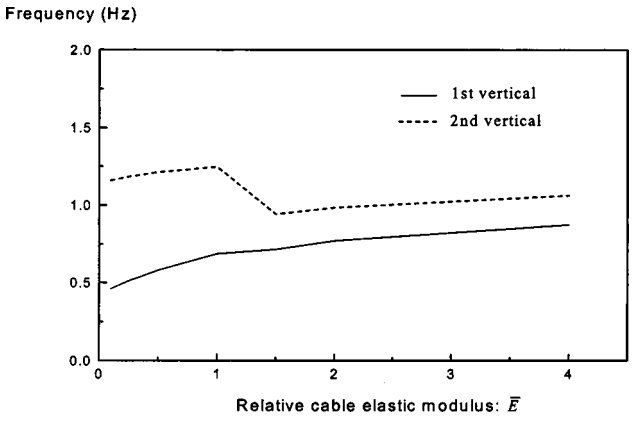


Fig. 8. First two vertical frequencies versus cable elastic modulus

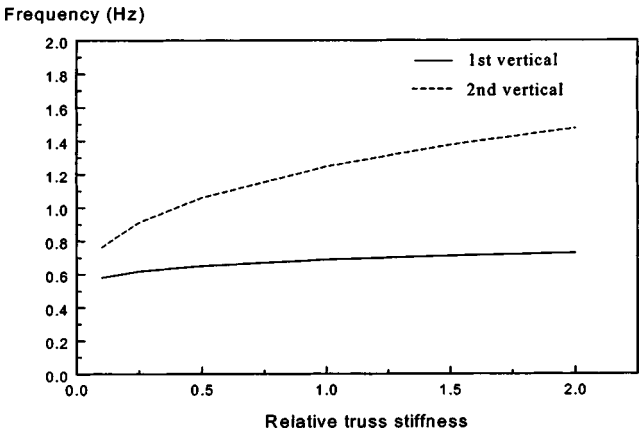


Fig. 9. First two vertical frequencies versus truss stiffness

self-weight, cable tension stiffness, suspender tension stiffness, the stiffness of the stiffening trusses, and vertical and transverse bending stiffness of the deck.

For cables, the cable tension stiffness depends on both the cross-sectional area A and elastic modulus E. Incrementing the cable cross-sectional area implies a larger tension stiffness, which is supposed to increase the frequencies. However, the cable weight increases proportionately, which results in reducing the frequencies. These two effects tend to cancel each other, resulting in frequencies that remain essentially unchanged.

Both transverse and vertical frequencies increase smoothly with increasing cable elastic modulus, as shown in Fig. 8, in which the relative cable elastic modulus $\bar{E}$ is defined by $\bar{E}=E/E_0$ where E_0 is the basic elastic modulus of the deck used in the initial model. The exception is in the range of $\bar{E}=1.0-1.5$ for the second vertical (the first asymmetric) mode. This observation is also true for the third vertical (the second symmetric) mode. In addition, variation in the elastic modulus of cables as well as cable cross-section area resulted in a reordering of the dominant mode shapes as they relate to the sequential order of natural frequencies.

It has been observed that the vertical frequencies increase smoothly when the suspender stiffness increases though almost no variation in the transverse frequencies was found. These results are consistent with the observation that suspenders of a suspension bridge provide stiffness in its geometric plane, which is vertical for the Roebling bridge.

For the stiffener trusses, both transverse and vertical frequencies increase with increasing stiffness, as shown in Fig. 9, especially for the higher modes. A reduction in truss stiffness leads to modal reordering. Mode numbers of the torsion and higher numbered vertical modes increase for the large truss stiffness models.

Results reported in Ren et al. (2003) demonstrate that the vertical bending stiffness (moment of inertia) of the deck does not contribute to either transverse or vertical frequencies, even though the deck vertical bending stiffness is increased fivefold. This result is consistent with the fact that the deck design does not provide vertical bending stiffness to the whole bridge. However, increasing the lateral bending stiffness moment of inertia of the deck does increase the transverse frequencies, as shown in Fig. 10, but does not contribute to vertical frequencies as anticipated. A variation in the lateral bending stiffness of the deck also leads to a reordering of the dominant mode shapes in the sequential order of natural frequencies given in Table 6.

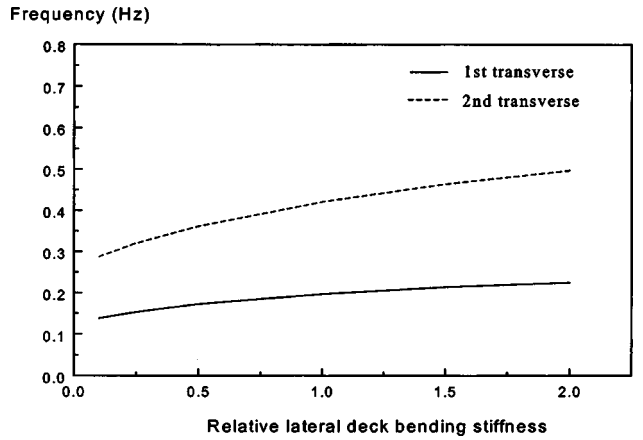


Fig. 10. First two transverse frequencies versus deck lateral bending stiffness

Conclusions

A complete 3D FE model has been developed for the J. A. Roebling suspension bridge in order to start the evaluation of this historic bridge. From the dead-load static analysis, the prestressed modal analysis, and parametric studies, the following conclusions and comments are offered:

1. The static analysis of a suspension bridge is geometrically nonlinear due to the cable sagging effect. Stress stiffening of cable elements plays an important role in both the static and dynamic analysis of a suspension bridge. Nonlinear static analysis without stress stiffening leads to an aborted computer analysis due to divergent oscillations in the solution. Large deflection analyses have demonstrated that this effect on the member forces and deck deflection under dead loads is minimal. Upon introducing proper initial strains in the cables, the static analysis of the Roebling suspension bridge can be based on elastic, small-deflection theory.
2. It has been demonstrated that a suspension bridge is a highly prestressed structure. Furthermore, all dynamic analyses must start from the deformed equilibrium configuration due to dead loading. It has been clearly shown that self-weight can improve the stiffness of a suspension bridge. In the case of the Roebling suspension bridge, the transverse (lateral) stiffness increases are much more significant than are in-

creases in the vertical stiffness. Inclusion of dead-load effect resulted in transverse natural frequency increases of nearly 20%, but the vertical natural frequencies only increased by approximately 5%.

3. Dominant modes for the Roebling suspension bridge in the low-frequency (0–1.0 Hz) range have been shown to be in the transverse direction; the lowest transverse frequency is about 0.19 Hz. This illustrates that the lateral stiffness is relatively weak: only a single truss is used in the Roebling bridge.
4. Throughout the parametric studies, the key parameters affecting the vertical modal properties of the Roebling suspension bridge are mass, cable-elastic modulus, and stiffening truss stiffness. Key parameters affecting the transverse modal properties are mass, cable-elastic modulus, stiffening truss stiffness, and the deck system transverse-bending stiffness. Stiffness parameter variations have been shown to cause some reordering in the sequencing of the natural modes of vibration. FE model updating is carried out in the companion paper (Ren et al. 2004) by adjusting these design parameters so that the live-loaded analytical frequencies and mode shapes match the ambient field test frequencies and mode shapes.
5. It is observed that the effect of decreasing the truss or cable stiffness by 50% does not lead to a significant decrease in the bridge natural frequencies. This fact points to the importance of the cables in governing the stiffness of a suspension bridge.

References

Abdel-Ghaffar, A. M. (1978). ''Free lateral vibrations of suspension bridges.'' *J. Struct. Div. ASCE,* 104(3), 503–525.

Abdel-Ghaffar, A. M. (1979). ''Free torsional vibrations of suspension bridges.'' *J. Struct. Div. ASCE,* 105(4), 767–788.

Abdel-Ghaffar, A. M. (1980). ''Vertical vibration analysis of suspension bridges.'' *J. Struct. Eng.,* 106(10), 2053–2075.

Abdel-Ghaffar, A. M., and Nazmy, A. S. (1991). ''3-D nonlinear seismic behavior of cable-stayed bridges.'' *J. Struct. Eng.,* 117(11), 3456–3476.

Abdel-Ghaffar, A. M., and Rubin, L. I. (1982). ''Suspension bridge response to multiple support excitations.'' *J. Eng. Mech. Div.,* 108(2), 419–435.

ANSYS User's manual; revision 5.6. (1999). Swanson Analysis Systems, Houston, Pa.

Boonyapinyo, V., Miyata, T., and Yamada, H. (1999). ''Advanced aerodynamic analysis of suspension bridges by state-space approach.'' *J. Struct. Eng.,* 125(12), 1357–1366.

Brownjohn, J. M. W., and Xia, P. Q. (2000). ''Dynamic assessment of curved cable-stayed bridge by model updating.'' *J. Struct. Eng.,* 126(2), 252–260.

Friswell, M. I., and Mottershead, J. E. (1995). *Finite element model updating in structural dynamics*, Kluwer Academic, Dordrecht, The Netherlands.

Grimes, R. G., Lewis, J. G., and Simon, H. D. (1994). ''A shift block Laanczos algorithm for solving sparse symmetric generalized eigenproblems.'' *SIAM J. Matrix Analysis Applications,* 15(1), 228–272.

Hazelet and Erdal. (1953). ''Report on inspection of physical condition of the Covington & Cincinnati suspension bridges over the Ohio River.'' Cincinnati.

Lall, J. (1992). ''Analytical modelling of the J. A. Roebling suspension bridge.'' MS thesis, Dept. of Civil and Environmental Engineering, Univ. of Cincinnati, Cincinnati.

Nazmy, A. S., and Abdel-Ghaffar, A. M. (1990). ''Three-dimensional nonlinear static analysis of cable-stayed bridges.'' *Compos. Struct.,* 34(2), 257–271.

Parsons Brinckerhoff Quade & Douglas, Inc. (1988). ''Bridge inspection report: John A. Roebling bridge over the Ohio River at Covington.'' *Division of Maintenance,* Dept. of Highways, Kentucky.

Ren, W.-X. (1999). ''Ultimate behavior of long span cable-stayed bridges.'' *J. Bridge Eng.,* 4(1), 30–37.

Ren, W.-X., Harik, I. E., Blandford, G. E., Lennet, M., and Baseheart, T. M. (2003). ''Structural evaluation of the John A. Roebling suspension bridge over the Ohio River.'' *Research Rep. KTC-2003,* Kentucky Transportation Center, College of Engineering, Univ. of Kentucky, Lexington, Ky.

Ren, W.-X., Harik, I. E., Blandford, G. E., Lenett, M., and Basehart, T. M. (2004). ''Roebling suspension bridge. II: Ambient testing and live-load response.'' *J. Bridge Eng.,* 9(2), 119–126.

Ren, W.-X., and Obata, M. (1999). ''Elastic-plastic seismic behaviors of long span cable-stayed bridges.'' *J. Bridge Eng.,* 4(3), 194–203.

Spyrakos, C. C., Kemp, E. L., and Venkatareddy, R. (1999). ''Validated analysis of Wheeling suspension bridge.'' *J. Bridge Eng.,* 4(1), 1–7.

West, H. H., Suhoski, J. E., and Geschwindner, L. F., Jr. (1984). ''Natural frequencies and modes of suspension bridges.'' *J. Struct. Eng.,* 110(10), 2471–2486.

Wilson, J. C., and Gravelle, W. (1991). ''Modeling of a cable-stayed bridge for dynamic analysis.'' *Earthquake Eng. Struct. Dyn.,* 20, 707–721.

View publication stats